RSC Advances

ROYAL SOCIETY OF CHEMISTRY

www.rsc.org/advances

Effect of reactive organoclay on physicochemical properties of vegetable oil-based waterborne polyurethane nanocomposites

T. Gurunathan[1,2,*], Smita Mohanty[1,2], Sanjay K. Nayak[1,2]

[1]Advanced Research School for Technology and Product Simulation (ARSTPS), Central Institute of Plastics Engineering & Technology, Guindy, Chennai 600032, India

[2]Laboratory for Advanced Research in Polymeric Materials (LARPM), Central Institute of Plastics Engineering and Technology, Bhubaneswar 751024, India

*: *Corresponding To:*

T.Gurunathan,
Advanced Research School for Technology and Product Simulation (ARSTPS),
Central Institute of Plastics Engineering & Technology,
Guindy, Chennai 600032, India.
Email: juru001@gmail.com
Phone No: 0674 2742852, **Fax No:** 0674 2743863.

ABSTRACT

The environmentally friendly vegetable oil-based waterborne polyurethane-organoclay nanocomposites have been successfully synthesized from castor oil polyols, isophorone diisocyanate, dimethylolpropionic acid. WAXD and TEM results showed that the addition of C30B contains a hydroxyl group led to the nearly exfoliated structures in WPUs. The thermal and mechanical properties of the nanocomposite films have been carefully investigated by FT-IR, DMTA, DSC, TGA, and tensile tests. As the C30B loading-level increased from 0 to 2%, the tensile strength and Young's modulus of the nanocomposites increased 16.7 to 27.9 MPa and from 22.3 to 134.8 MPa, respectively. The enhanced mechanical and thermal performance was primarily attributed to the formation of the strong interfacial interactions between filler and matrix. Morphological changes induced by the addition of clays were analyzed using rheological results. This work produced new nanocomposites derived from castor oil polyols with a high-biomass content, and Its high performance could contribute to a sustainable chemical industry.

1. Introduction

Polymer from vegetable oil-based renewable resources has received much attention during the past few decades, due to strict petroleum resources and environmental legislation.[1] Polyurethanes (PUs) are among the most versatile polymeric materials which offer a wide range of applications, such as coatings, binders, adhesives, elastomers, packaging materials and for automotive finishes.[2-5] However, conventional (PUs) products usually contain a significant amount of organic solvents and sometimes even free isocyanate monomers.[6] For this reason, waterborne polyurethane (WPU) has received much attention due to its zero or low volatile organic compounds (VOCs). This has led to increased efforts to formulate waterborne PUs for use as coatings, adhesives, and related end uses.[7,8] Waterborne coatings have many advantages relative to conventional solventborne coatings, including excellent adhesion, hardness, flexibility, general chemical resistance, gloss, and weatherability.[9,11] Because of these properties, aqueous polyurethane dispersions (PUDs) are one of the most rapidly growing and active branches of polyurethane (PU) Chemistry and Technology.[12] The added advantage of PUDs is that the viscosity of the coherence is independent of molecular weight of the polymer. Moreover, PUDs can be prepared at high solid content with a molecular weight high enough to form films with excellent quality simply by physical drying.

WPU dispersions are considered as a two-phase colloidal system in which polyurethane particle are dispersed in water (continuous phase).[13] They consist of PU backbones with some pendant acid or tertiary nitrogen groups, which are partially neutralized or quaternized, respectively, to form salts, and these centers are responsible for water dispersibility.[14] Parameters such as selection of isocyanate, types of ionomers, and types of polyols affect the performance of the resulting waterborne PUDs. The relative merits and demerits are of these aqueous ionic

polymers are of great research interest and were discussed by some authors.[15-17] However, waterborne polyurethanes have a disadvantage in that the PU films exhibit high hydrophilic properties due to the presence of the hydrophilic carboxylate groups in the main chain, resulting in poorly mechanical properties and water or solvent resistance.[18] For the purpose of improving the properties of WPU, several modifications have been researched; polymer hybridizing with organic and inorganic oxides such as starch,[19] casein,[20] silica,[21] titania,[22,23] and clay[24-26] have been used to improve toughness and elasticity. Among these methods, reacting the carboxylate groups in the PUDs with a clay represent perhaps most convenient methods, because it can decrease the extent of phase separation or increase the compatibility of the polymer filler interaction.[27] Moreover, most of the waterborne PU-nanocomposites were prepared in organic solvents.[28] Herein, nanocomposites demonstrate more meaningful to the environment and would have great potential applications in the future.

Environmental protection can be better understood when the polyol is replaced with renewable sources, such as some vegetable oils, to synthesize the waterborne urethane materials. Among many kinds of vegetable oils, the castor oil possessing three hydroxyl groups (–OH) is a superb candidate for the synthesis of WPU. In view of both environmental conservation and adequate utilization of renewable resources, we thus, in this work, attempted to use castor oil (CO) to synthesize a WPU in order to obtain economically viable materials. In the present investigation, organically modified nanoclay Cloisite 30B (C30B) has been blended with castor oil-based anionic PUDs to obtain self-curable PU dispersions. The castor oil-based PU is chemically bonded with C30B clay and the crosslink density of the nanocomposites in increased substantially. Through applications of this way, thermo-stability, hardness, water or solvent

resistances of nanocomposite films are increased substantially. This work provides an effective and promising way to prepare biorenewable sources, high-performance coating materials.

2. Experimental

2.1. Reagents and Materials

Castor oil was of commercial grade and purchased at a local supplier (Ramcharan Oil mill, Hyderabad) and used directly without further purification. Isophorone diisocyanate (IPDI: Z and E isomer in 3:1 ratio), 2,2-bis(hydroxymethyl) propionic acid (bis-MPA), isophorone diamine (IPDA), dibutyltindilaurate (DBTL) were purchased from Aldrich (Milwaukee, WI). Triethylamine (TEA) and acetone (dried over 4Å molecular sieves) was purchased from S.D. Fine chemicals (Mumbai, India) and the other reagents were used as received without further purification.

The reactive clay, Cloisite® 30B (C30B, 90 mequiv./100 g) a montmorillonite clay modified with a quaternary ammonium salt, was procured from Southern clay Products (Gonzales, TX, USA). The quaternary ammonium ion has a structure, N^+ $(CH_2CH_2OH)_2$ (CH_3) T (methyl, tallow, bis(2-hydroxyethyl)), Where N^+ represents quaternary ammonium chloride, and T denotes tallow consisting of ca. 65% C_{18}, ca. 30% C_{16} and ca. 5% C_{14}.[29] The organoclay intrinsically contained approximately 2 wt% moisture, which was removed by drying in a vacuum oven at 80 ^oC for 24 h. However, during experiments, the clay reabsorbed approximately 0.30 wt% moisture at room temperature in a room with 50% relative humidity during this period.

2.2. Synthesis of the Castor oil-based Waterborne Polyurethane-C30B Nanocomposites (WPU-C30B)

Scheme 1 represents the method and conditions of synthesis of castor oil-based WPU-C30B nanocomposites. The castor oil, IPDI and 0.01% of DBTDL as catalyst were charged to a

moisture-free four-necked flask equipped with a mechanical stirrer, nitrogen inlet, condenser, and thermometer. The flask was heated at 75-80 ^{o}C for nearly 1-2 h with vigorous overhead stirring. During this time isocyanate (–NCO) content, was monitored at constant time intervals by standard N-dibutylamine back titration method. Upon reaching the theoretical –NCO value, the calculated amount of hydrophilic monomers (bis-MPA) and 0.01% drop of DBTDL were added and maintained at 60 ^{o}C until the proper –NCO value was obtained. The mole ratio of the –NCO groups of the IPDI, the –OH groups of the castor oil, and the –OH groups of the bis-MPA was kept at the ratio of 2:1:09. The reaction was further carried out at 75 ^{o}C for 1 h, and then 50 mL acetone was added to adjust the viscosity and prevent gelation. The reaction end point was confirmed by FT-IR spectra for the disappearance of the peak at 2270 cm^{-1} corresponding to stretching vibration of the –NCO group. After cooling the reaction mixture to room temperature, the PU prepolymers were neutralized by TEA (three equiv. per bis-MPA) and stirred for 30 min. The C30B was added and allowed to react with the excess amount of –NCO groups at 25 ^{o}C for 1 h. Formation of the WPU-C30B nanocomposites was accomplished by slowly adding the water to the neutralized acetone solution of the PU prepolymers at ambient temperature with an agitation speed of 500 rpm. The above dispersion was transferred to a rotary evaporator, and the acetone was removed to afford, castor oil-based WPU-C30B nanocomposite dispersions were formed with about 30 wt% of solid content. The structure of the synthesized castor oil-based polyurethane prepolymer (PUP) was further supported by ^{1}H and ^{13}C NMR spectroscopy analyzes (Fig. S1 and S2) with details as follows:

^{1}H NMR (400 MHz, $CDCl_3$): δ (ppm) 0.81(t, 9H,–CH_3), 1.40 (q, 8H, –CH_2), 2.05 (q, 18H, –CH_2), 2.8(d, 6H,–CH_2–), 2.92(t, 6H, –CH_2–), 3.21(m, 3H, –CH–), 3.56(s, 2H,–CH_2–N),

4.10(p, 3H, –CH–O), 4.34(d, 2H, –CH_2–O), 4.63(d, 1H, –NH–), 5.21(t,1H, –CH–O), 5.41(d, 6H, –HC=CH–).

^{13}C NMR (400 MHz, $CDCl_3$): δ (ppm) 12.3, 21.1, 23.0, 25.2, 27.0, 29.3, 30.1, 32.5, 33.9, 35.1, 36.2, 37.3, 47.8, 57.1, 62.8, 69.3, 71.4, 75.6, 125.8, 134.1, 156.2, 157.5, 173.26, 207.8.

Specifically, 0.5, 1 and 2 wt% of C30B were added to the PU prepolymer solutions to study the influence of C30B content on reactivity. The nomenclature used for the resulting nanocomposites is as follows: a nanocomposites containing 0.5, 1, and 2 wt% of C30B is designated as WPU-C30B0.5%, WPU-C30B1%, and WPU-C30B2%, respectively. For comparison, the sample without C30B was also prepared, and the residual isocyanate reacted with water to form amines, which can then react with the remaining isocyanate to form a polyurea. This control sample is designated as WPU-C30B0. The preparation of nanocomposite dispersions film is reported by Gurunathan et al.[30]

2.3. Attenuated total reflection-Fourier-transform infrared (ATR-FTIR)

ATR-FTIR spectroscopy was used to identify the functional groups of the WPU and their nanocomposites using a ThermoScientific Nicolet^{TM} 6700, USA. Spectra were obtained at 4 cm^{-1} resolution and number of scan 32 in the standard wavenumber range from 400 to 4000 cm^{-1}.

2.4. Nuclear magnetic resonance (NMR)

The ^{1}H and ^{13}C nuclear magnetic resonance (NMR) of the synthesized samples were preserved in a Bruker Avance-400 MHz spectroscopy by using tetramethylsilane (TMS) as standard at room temperature, and samples were dissolved in deuterated chloroform ($CDCl_3$) as solvent.

2.5. Transmission electron microscopy (TEM)

The dispersibility of the clay layers in the samples was examined with a transmission electron microscopy (TEM) (JEM 1400 TEM mode, JEOL, Japan) at an accelerated voltage of 100 kV.

The ultrathin sections (60-80 nm in thickness) were cryogenically sliced at -80 to -100 ^{o}C using a Cryo Leica EM UC6 instrument (Leica Microsystems, Switzerland) with a diamond knife and viewed without staining.

2.6. Wide angle X-ray diffraction (WAXD)

WAXD analysis was conducted for all nanocomposites to study the extent of intercalation and exfoliation behavior of nanoclays within the polymer matrix using a Shimadzu X-ray diffractometer 7000 L, Japan, (graphite monochromator Cu Kα radiation with $\lambda = 0.15406$ nm) at a scanning rate of 0.5^{o}/min within a range from 1^{o} to 10^{o}. The basal spacing of the clay, d, was calculated using the Bragg's equation, $\lambda = 2d \sin \theta$.

2.7. Differential scanning calorimetry (DSC)

DSC was performed on a thermal analyzer (DSC, Q200, M/s TA Instruments USA). Sample of ~3 mg was heated at a rate of 20 ^{o}C/min from 25 to 200 ^{o}C to remove the thermal history, equilibrated at -70 ^{o}C and then heated to 200 ^{o}C at a rate of 10 ^{o}C/min. Two measurements were performed for each sample.

2.8. Thermal gravimetric analysis (TGA)

Thermogravimetric analyzer (TGA, Q500, TA Instruments, USA) was used to measure the weight loss of the films under an air atmosphere. The samples (~7mg) were scanned from 0 to 600 ^{o}C at a heating rate of 10 ^{o}C/min in a nitrogen environment with purge flow of 20 mL min^{-1}. The maximum rate of degradation was observed from the derivative thermogram (DTG). Two determinations were done on each sample.

2.9. Dynamic mechanical thermal analysis (DMTA)

DMTA behavior of the nanocomposite films was examined in a DMTA IV instrument (Rheometric Scientific, United States) operated in a multifrequency strain mode, using a single-

cantilever clamp, in accordance with the standard ASTM D4065. The viscoelastic properties were measured under a nitrogen atmosphere, at a heating rate of 5 ^{o}C/min from -50 to 100 ^{o}C and a frequency of 1 Hz. Rectangular Samples were cut into dumbbell shapes, and two replicates were performed for each sample.

2.10. Rheological properties

A modular advanced rheometer (MARS III, Thermo Fisher Scientific, Germany) was used for rheological measurements under oscillator mode with a 25 mm diameter parallel plate fixture. Dynamic storage modulus (G') and complex viscosity ($|\eta^*|$) were measured from 0.1 to 100 rad/s a fixed strain of 0.04. The experiment was performed at 190 ^{o}C using a gap width of 1 mm.

2.11. Mechanical properties measurement

Tensile properties, such as tensile strength, tensile modulus and elongation at break, were measured in accordance with the ASTM D638 using specimens of dimensions 80 ×10 mm^2 (length × width) at a crosshead speed of 5 mm/min and gauge length of 50 mm in the Universal testing machine, (UTM, Instron 3386, UK). The testing was carried out in standard laboratory conditions of 23±5 ^{o}C+55-/.RH. The toughness of the polymer was obtained from the area under the corresponding tensile stress-strain curves. Five replicates of each sample were taken, and the average value of tensile properties are reported.

3. Results and discussion

3.1. Characterization of nanocomposites by FT-IR

FT-IR spectroscopy is widely used as a convenient technique to study the strength and extent of hydrogen bonding in PUs. In Fig. S3, the C30B exhibit –CH stretching peaks at 2970 and 2880 cm^{-1}, which correspond to hydrocarbon chains of the organic ammonium ions present in treated C30B clay. The possibility of urethane linkage formation between –CH_2CH_2OH functionalities

of C30B and isocyanate (N=C=O) end groups of polymer chains was investigated by real-time ATR-FTIR is shown in Fig. 1. The presence of the following characteristic bands supports the structure of the synthesized WPU. The broad band around 3335–3400 cm^{-1} arises which shows the stretching vibration of –N–H bond in the urethane segments (–NHCOO). The peak at 2800–3000 cm^{-1} is due to the –CH stretching vibrations (asymmetric $–CH_3$ stretching: 2972 cm^{-1}; asymmetric $–CH_2$ stretching: 2920 cm^{-1}; symmetric $–CH_3$ stretching: 2885 cm^{-1} and symmetric $–CH_2$ stretching: 2869 cm^{-1}), peak in between 1665–1780 cm^{-1} is due to the amide I: –C=O stretching vibrations. The peak at 1528–1419 cm^{-1} (amide II: $\delta_{N–H} + \nu_{C–N} + \nu_{C–C}$; sensitive to chain conformation and intermolecular hydrogen bonding),[31] 1372–1381 cm^{-1} ($\nu_{C–N}$), 1252–1256 cm^{-1} (amide III, $\nu_{C—N}$, N–H bending and C–Cα), 767–771 cm^{-1} (amide IV; N–H out-of-plane), 695 cm^{-1} (amide V).[32] One of the primary concerns is the reactivity of clay with N=C=O group of the prepolymer. The primary bands in PUs, the –N–H stretching as a proton donor and the carbonyl stretching as a proton acceptor are sensitive to hydrogen bonding. Fig. 2 shows the expanded amide I and –NH zone in the range of 1600-1800 and 3000-3700 cm^{-1} respectively. The investigation of structure-property relationships in polyurethanes has gained a unique importance due to their ability to form hydrogen bonds between —NH and —C=O groups of urethane/urea or ester/ether segments.[9] Thus, by analyzing these zones, one can get better information regarding the extent of hydrogen bonding present in the polymer. By comparing the peak shifting of —NH and —C=O zone, for WPU-C30B0 and WPU-C30B nanocomposites at different clay contents is shown in Fig. 2.

To confirm the reactivity of clay with PU, we tested the hybrid composite using FT-IR spectra at different stages of the reaction (Fig. 2). In the reactive nanocomposite, the peak intensity for –NCO group at 2270 cm^{-1} slightly decreased with increasing time, which confirmed that

significant reaction had occurred between –OH group of C30B and –NCO group of prepolymer in castor oil-based WPU-C30B nanocomposite.[33] This is due to the more interaction between the C30B surface hydroxyl groups and –NCO group of PU prepolymer (shown in Scheme 2), which disrupts the phase separation phenomenon and thus decreases the hard phase formation in the PU matrix. The disruption of the phase separation phenomenon with increasing C30B content is due to the C30B surface geometry which constrains the –NH groups of the hard segments in the reacting PU prepolymer to form hydrogen bondings with the other hard segment –C=O groups [i.e., –N–H····O=C–]. Thus, there is a more possibility of formation of phase mixing structures with increasing the C30B content [i.e., —N—H····O—C(=O)—].[32] However, all hydroxyl groups could not participate in cross-linking reaction due to steric hindrance. The broad peak at 3560 cm^{-1} some unreacted hydroxyl groups of C30B in this system.

3.2. Morphology of different WPU-C30B nanocomposites

Morphology of the dispersed layers is important in determining the properties of the final coatings. To investigate the surface morphology of the dispersed layers, the films were characterized by TEM. The representative TEM micrographs for WPU-C30B0 and WPU-C30B nanocomposites were presented in Fig. 3. Usually, several factors, such as the hydrophilicity, ionic group position, prepolymer viscosity, and the chemical structure of the soft segment, play a key role in influencing the particle size of the PU dispersion.[34,35] It is well known that the efficiency of the nanoclay in improving the properties of hybrid materials mainly depends on their degree of dispersion in the polymer matrix.[30] The TEM micrographs suggest that the nanoclay are well dispersed in the PU matrix in case of lower clay content, whereas some cluster-like structures are formed at higher label of clay loading. The size and number of these particles increased with increase of clay wt% in the nanocomposite. However, clay platelets were

randomly oriented in WPU-clay nanocomposite. In general, the particle size of the WPU dispersion is governed by the hydrophilicity of the ionomer.[35,36] The mean particle size was increased in the dispersion with increasing of hydrophobic clay content indicates the inclusion of the clay layer in the dispersion. It is also observed that the WPU and their clay layers are more or less homogeneously assembled in the film (Fig. 3). The above consideration that some of the hydroxyl groups in C30B may interact with carbonyls in the hard segments resulting in slightly less ordering of hard domains. This is manifested in the TEM images where the dispersion of clay C30B is very good through all the phases. This kind of interaction between carbonyls and hydroxyls of C30B was already mentioned in the previous study by pattanayak and Jana.[29] The dispersion clay layers, which have an original thickness around 1 nm, average length 80-100 nm and average interlayer distance of 60-100 nm. The size of some of the clay layers appears to reach about 130 nm in length owing the hydroxylated edge-edge interaction of clay layers.

3.3. X-ray Diffraction of different WPU-C30B nanocomposites

WAXD measurements were taken further to confirm the dispersion behavior of WPU-C30B nanocomposites. Fig. S4 displays the WAXD patterns in the range of 2θ =1-10^{o} for a neat C30 as well as for WPU-C30B nanocomposites films. The neat C30B shows an intense diffraction peak centered at 2θ =4.82 corresponding to the basal spacing of 1.82 Bragg reflection planes.[37] The strong diffraction peak disappears in the WXRD pattern of the nanocomposite films. The disappearance of the WAXD peak suggests that the polymer chains are intercalated between the layers of organoclay and induced delamination of the organoclays, which resulted in the high disordered nanoscale dispersion of the organoclay throughout the WPU-C30B films.[38] This means that the homogeneous dispersion of C30B within PUP is attributed to the presence of strong hydrogen bonding interactions between –C=O groups of polyurethane –OH groups in

C30B as reported in the previous studies.[39] From the FT-IR observation as discussed above, the hydrogen bonding interactions between polyurethane chains and the organoclay increased [see Fig. 2]. The TEM results further confirm that C30B was in an intercalation state in PUP (Fig. 3). On the basis of these observations, it can be assumed that the degree of delamination of the organoclay in the PU is dependent on the degree of shear during the affinity of PUP chains with the surface of an organoclay.

3.4. DSC analysis of different WPU-C30B nanocomposites

The waterborne PU and their hybrid nanocomposites were characterized by recording the DSC profiles (Fig. S5). All of the curves show one-glass transition temperature (T_g), indicating the amorphous nature of these castor oil-based WPU and their hybrids, which is in good agreement with the FT-IR results. Comparison of T_g values of WPU-C30B0, WPU-C30B nanocomposites (Table 1) show that composites have higher glass transition temperatures, with an of around 17 ^oC, when the clay proportion increases from 0 to 2 wt%. This fact can be explained by the polymer chain motion being restricted at higher crosslink densities and the increased free volume of the nanocomposites as mentioned earlier. However, the WPU film with a variety of C30B loading have almost similar T_g, presumably because the soft chains from the C30B compensate for the increased crosslink densities.[40,41] Similar behavior has been reported in the literature by Fu et al.[42] prepared PU/polyhedral oligomeric silsesquioxanes (POSS) nanocomposites based on diphenylmethane-4,4-diisocyanate and polytetra methylene glycol were synthesized using a mixture of POSS-diol and 1,4-butanediol as chain extenders. They found that the increase of the POSS concentration was found to reduce the microphase separation between the domains and increase the T_g of the soft segments. The T_g obtained from DMTA are higher than the T_g obtained from DSC. This results from the different nature of these two

methods. DMTA measures the change in the mechanical response of the polymer chains, while DSC measures the change in heat capacity from frozen to unfrozen chains.[43]

3.5. TGA analysis of different WPU-C30B nanocomposites

The thermal behavior of the neat WPU films, as well as nanocomposite, was studied by TGA. Fig. 4(a) shows the TGA curves of WPU-C30B0 and WPU-C30B nanocomposites with different clay loading, and the TGA data such as 10 wt% loss temperature ($T_{10\%}$), 50 wt% loss temperature ($T_{50\%}$) and maximum decomposition temperature (T_{max}) as listed in Table 2. In general, polyurethanes exhibit relatively low thermal stability because of the presence of labile urethane bonds, which decompose below 300 ^{o}C, depending upon the isocyanate and polyols employed. [44] The TGA curve of the WPU-C30B0 has two-weight loss stages and WPU-C30B nanocomposites show three distinct weight loss stages. The TGA data, as reported in Table 2, suggests that the thermal stability of the blended films is higher than the neat polymer and its increases with increasing the clay content. The enhancement of thermal stability is possible by formation of stable ether linkages due to the interaction between the two adjacent –OH groups in case of WPU-C30B. These results indicate that the well intercalated C30B layers serve as a thermal insulator and mass transport barrier to the volatile products created during decomposition and thus increase the degradation temperature. Greater thermal stability for these types of modified clays has also been reported by Wang et al. due to strong covalent bond formation between the urethane linkages and the modified montmorillonite.[45] The thermal enhancement usually depends on the dispersion and the degree of delamination, which results from the proper clay chemical modification and polymer-particle interactions. The high residual mass of the nanocomposites compared to the neat samples, at high temperature, mainly comes from the inorganic silica part of C30B organoclay. Similar results have been reported by Cao et al.[46] for a

Polycaprolactone-based WPU/cellulose nanocrystal (CN) nanocomposite. In this paper co-crystallization phenomenon induced the formation of a co-continuous phase between the filler and matrix which notably increase the interfacial adhesion and consequently contributed to a development in the thermal stability of the nanocomposites.

The derivative thermogram (DTG) curves clearly indicate a three-step degradation profile with an initial decomposition temperature around ~250 ^{o}C (Fig. 4(b)). The smaller weight loss temperature around ~150 ^{o}C is might be due to the evaporation of absorbed moisture in the dispersion films. For an instant, the first-weight loss stage, in the temperature range of 150-300 ^{o}C, is due to the dissociation of the urethane bonds to form isocyanates, alcohols, primary and secondary amines, olefins, and loss of carbon dioxide from the urethane bond.[44] The second-weight loss stage, in the temperature range of 300-400 ^{o}C, are attributed to castor oil chain scission. The last degradation step above 500 ^{o}C corresponds to the decomposition of organically molecular chains from functionalized clay and remnant polyurethane.[47]

3.6. DMTA analysis of different WPU-C30B nanocomposites

The incorporation of clay has a significant impact on the dynamic mechanical properties of the castor oil-based WPU-C30B nanocomposites. To investigate the influence of nanocomposites are examined by DMTA measurements. The storage modulus (E') and dissipation factors (tan δ) curves as a function of temperature for the synthesized neat polyurethane and the nanocomposite films with different clay loadings as shown in Fig. 5(a) and (b), and the glass transition temperature as summarized in Table 1. As can be seen in Fig. 5(b), a plateau appeared in storage modulus values, which presented higher E' values with increasing the clay content, comparing with the values obtained for WPU. As the temperature increases, the E' values of all PU film decreases slightly until a sharp decrease is observed. This decrease in E'

value corresponds to an energy dissipation shown in the tan δ -temperature curve, where a maximum, taken as the T_g, is observed in the tan δ curve (α relaxation).[48,49] Then, at higher temperatures, the E' storage modulus reaches a rubbery plateau, assigned to the glass–rubbery transition, suggesting the nature of the crosslinking. Moreover, a sharp drop in E' is noted at about 50 ^{o}C, associated with the glass transition. Above the melting point, E' of the nanocomposite film modified by the clay is still considerably higher than that of WPU. Also, inconspicuous dissipation of E' after 120 ^{o}C can be seen in the case of the WPU, which might be associated to the hard domains transition (Fig. 5(b)).[50] However, the dissipation tends to diminish or even disappear with increasing of the clay content. It might be due to the further phase separation caused by the incorporation of the clay, which leads to decreasing the interplay between the soft segments and hard segments. As a result, the temperature of the hard domains transition shifts to a higher one.

The tan δ vs temperature curves of the WPU-C30B0 and WPU-C30B nanocomposites films as presented in Fig. 5(a). It can be recognized that the T_g of the nanocomposite slightly shifted to the higher temperature from 53.08 to 63.09 ^{o}C with increasing the clay content from 0 to 2 wt%. It can be connected to the incorporation of the clay that increased the interaction between the soft segments and hard segments, as mentioned previously. The peak height of tan δ curve tends to decrease with the presence of clay, caused by the improvement of the crosslink density in polymer matrixes and the mobilization of the PU chains.[51] However, greater loading of clay content can lead to the aggregation of clay to jeopardize the film properties of nanocomposites, resulting in the increase of the peak intensity when the clay content is more than 2 wt% (Fig. 5(a)). In addition, similar behavior was observed for all the PU/POSS nanocomposites regardless of the concentration of POSS, suggesting that the incorporation of POSS did not significantly

alter the E' and tan δ of PUDs. The reason may be due to the relatively poor solubility of neat POSS in NMP, and, therefore, the polymerization reaction might not have proceeded to completion as expected.[52]

3.7. Rheological behavior of different WPU-C30B nanocomposites

Dynamic melt rheological property was investigated to observe the melt processability of the synthesized nanocomposites. The angular frequency dependence of both complex viscosity ($|\eta^*|$) and storage modulus (G') of all samples in the molten state are shown in Fig. 6. The $|\eta^*|$ and G' increased substantially with the increase of clay content, and the values were higher in the case of WPU-C30B nanocomposites, which was ascribed to the formation of C30B crosslinking network that make the mobility of the polymer chains more difficult, and relatively higher molecular weight of WPU-C30B nanocomposites. This improvement can be explained on the basis of resistance to flow and deformation of the molten polymer chain imposed by clay particles as shown in Scheme 3. It is reported that the presence of cross-links or entangled networks in the polymer melt could increase the modulus and viscosity.[53] The cross-link density is related to the amount of C30B clay present; as the amount of clay increases, the cross-link density increases. The results suggest that the behavior of clay can facilitate cross-linking reaction, and thereby cross-linking density is increased.[54] In addition, the adsorption of WPU chains onto the surface of C30B clay can also result in a rise in the effective cross-linking.[55] Similar behavior with higher slope for better clay dispersion was previously observed for poly(lauryl lactam)-adipic acid-poly(tetramethylene ether) glycol block copolymer/organoclay nanocomposites[56] and a poly(ethylene-*ran*-vinyl acetate-*ran*-vinyl alcohol)/organoclay nanocomposite.[57] The above observation supports the results of the WXRD patterns (Fig. S4.).

3.8. The effects of C30B on the mechanical properties of WPU-C30B nanocomposites

Typical tensile stress-strain curves for the WPU-C30B0 and WPU-C30B nanocomposites with different clay content as shown in Fig. S6. The corresponding tensile properties, namely Young's moduli, the tensile strength, and the tensile elongation of the nanocomposites, are summarized in Table 2. The castor oil-based WPU-C30B nanocomposites with the formulation in this work are ductile materials. Upon the addition of clay from 0 to 2 wt%, Young's modulus increased to 134.8 MPa from 22.3 MPa. At the same time, the tensile strength is increased to 27.9 MPa from 16.7 MPa. On the other hand, the tensile elongation dropped significantly from 343.7 to 144.8%, with an increase in the crosslink density, as expected. An increased crosslink density increases the tensile strength but lowers the elongation at break.[58,59] These enhancements of mechanical properties are due to the interfacial interaction between clay and the WPU matrix resulting from hydrogen bonding interaction.[60] This interfacial bonding allows the load transfer capability from the ductile polymer to the strong continuous phase and reduce the slippage during straining. In addition, this interaction may be able to alter the static microphase morphology of the WPU in such a way that results in enhanced mechanical properties.[61] The measurements confirmed aggregation of clay as shown in the earlier TEM picture (Fig. 3). Because of the aggregation of the nanofillers, the filler-filler interaction is effective over the filler-polymer interaction. Also, aggregated particles act as defects. As a result, a decrease in the tensile strength is seen in the hybrid films. The mechanical behavior of the WPU-C30B nanocomposites is similar to what was reported earlier by Choi et al.[62] in their work on effect of the chain extender 2-hydroxyethyl acrylate (HEA), 1,4-butanediol (BD), and vinyltrimethoxysilane (VTMS) modified clay showed pronounced effect over natural clay in terms of tensile strength and thermal stability of the PUD films. The results showed that the vinyl

groups of VTMS form covalent bonds with the vinyl termini of PU by UV cure to synthesize WPU/clay hybrid nanocomposite.

4. Conclusions

Castor oil-based WPU-C30B nanocomposites have been successfully synthesized. It has been observed that the PUP chains are chemically bonded to the C30B to enhance the crosslink density of the nanocomposites, which is strong evidenced by the tan δ and the heat capacity change at T_g. The FT-IR study of –C=O and –NH zone suggests that there are higher hydrogen bonding interaction and network structure formation with increasing organoclay content. Areas under endothermic peaks and the onset temperature of soft segment movement in DSC thermograms were analyzed to examine the change in the morphology of nanocomposites. The ^{1}H and ^{13}C NMR spectra indicate the formation of castor oil based PUP and the TEM images show that C30B aggregates are reasonably well dispersed close to exfoliation in the WPU-C30B nanocomposites. With the increase in C30B content, the resulting films exhibit stress-strain behavior ranging from elastomeric polymers to ductile plastics and possess Young's moduli ranging from 22.3 to 134.8 MPa, tensile strengths ranging from 16.7 to 27.9 MPa, and % of elongation values ranging from 343. 7 to 144.8 %. The thermal and mechanical properties of these castor oil-based WPU-C30B nanocomposites films are comparable to or even better than those from petroleum-based polyols. Therefore, this work provides a useful and promising new way of using renewable sources to make environmentally friendly, vegetable oil-based polymers with high performance for coating and adhesive applications.

Acknowledgements

The authors are thankful to Department of Chemicals and Petrochemicals (DCPC), Ministry of Chemicals and Fertilizers, Government of India (GOI) for sponsoring the Project.

References

1 Y. Xia, R. C. Larock, *Green. Chem.* 2010, **12**, 1893–1909.

2 A. M. Youssef, *RSC Adv.*, 2014, **4**, 6811-6820.

3 K. M. Zia, H. N. Bhatti, I. A. Bhatti, *React. Funct. Polym.,* 2007, **67**, 675–692.

4 A. M. Youssef, M. S. Abdel-Aziz, S. M. El-Sayed, *Int. J. Biol. Macromol.* 2014, **69**, 185–191.

5 A. M. Youssef, M. F. Malhat, A. A. Abdelhakim, *Polym. Plast. Technol. Eng.* 2013, **52**, 228–235.

6 T. Gurunathan, C. R. K. Rao, R. Narayan, K. V. S. N. Raju, *J. Mater. Sci.*, 2013, **48**, 67–80.

7 B. U. Ahn, S. K. Lee, S. K. Lee, H. M. Jeong, B. K. Kim, *Prog. Org. Coat.,*2007,**60**,17–23.

8 Noble, K. -L., *Prog. Org. Coat.,* 1997, **32**, 131–136.

9 D. K. Chattopadhyay, K. V. S. N. Raju, *Prog. Polym. Sci.,* 2007, **32**, 352–418.

10 L. Lei, L. Zhong, X. Lin, Y. Li, Z. Xia, *Chem. Eng. J.,* 2014, **253**, 518–525.

11 N. R. Paluvai, S. Mohanty, S. K. Nayak, *Polym. Plast. Technol. Eng.*, 2014, **53**, 1723–1758.

12 S.G. Liu, G.Q. Zhu, *Eur. Polym. J.* 2007, **43**, 3904–3911.

13 D. J. Hourston, G. Williams, R. Satguru, J. D. Padget, D. Pears, *J. Appl. Polym. Sci.* 1998, **67**, 1437–1448.

14 S. Zhang, W. Miao, Y. Zhou, *J. Appl. Polym. Sci.,* 2004, **92,** 161–164.

15 B. K. Kim, J. C. Lee, *J. Polym. Sci. A.,* 1996, **34**, 1095–1104.

16 P. Krol, B. Krol, P. Holler, N. Telitsyna, *Colloid. Polym. Sci.,* 2006, **284**, 1107–1120.

17 Y. Chen, Y. L. *J. Appl. Polym. Sci.,* 1992, **46**, 435–443.

18 S. C. Wang, P. C. Chen, J. T. Yeh, K. N. Chen, *React. Funct. Polym.,* 2007, **67**, 299-311.

19 Q. Wu, L. Zhang, *Ind. Eng. Chem. Res.* 2001, **40**, 558–564.

20 N. Wang, L. Zhang, Y. Lu, *Ind. Eng. Chem. Res.,* 2004, **43**, 3336-3342.

21 H. H. Wang, Y. T. Lin, *J. Appl. Polym. Sci.* 2003, **90**, 2045–2052.

22 D. M. Wu, F. X. Qiu, H. P. Xu, D. Y. Yang, *Plast. Rubber. Compos.,* 2011, **40**, 449.

23 A. M. Youssef, S. Kamel, M. A. El-Samahy, *Carbohyd. Polym.* 2013, **98**, 1166–1172.

24 H.-C. Kuan, W.-P. Chuang, C,-C. M. Ma, C.-L. Chiang, H.-L. Wu, *J. Mater. Sci.,* 2005, **40**, 179– 185.

25 B. K. Kim, J. W. Seo, H. M. Jeong, *Eur. Polym. J.* 2003, **39**, 85.

26 H. Essawy, A. Badran, A. M. Youssef, A. E. A. El-Hakim, *Polym. Bull.,* 2004, **53**, 9–17.

27 H. Zou, S. S. Wu, J. Shen, *Chem. Rev.* 2008, **108**, 3893–3957.

28 K. K. Jena, K. V. S. N. Raju, *Ind. Eng. Chem. Res.* 2007, **46**, 6408.

29 A. Pattanayak, S. C. Jana, *Polymer,* 2005, **46**, 3275–3288.

30 T. Gurunathan, C. R. K. Rao, R. Narayan, K. V. S. N. Raju, *Prog. Org. Coat.,* 2013, **76**, 639-647.

31 M. M. Coleman, L. H. Lee, D. J. Skrovanek, P. C. Painter, *Macromolecules,* 1986, **19**, 2149–2157.

32 A. K. Mishra, D. K. Chattopadhyay, B. Sreedhar, K. V. S. N. Raju, *Prog. Org. Coat.,*2006, **55**, 231–243.

33 M. M. Rahman, H. J. Yoo, C. J. Mi, H. D. Kim, *Macromol. Symp.* 2007, **251**, 249–250.

34 B. S. Kim, B. K. Kim, *J. Appl. Polym. Sci.* 2005, **97**, 1961–1969.

35 S. H. Park, I. D. Chung, A. Hartwig, B. K. Kim*, Colloids Surf., A* 2007, **305**, 126–131.

36 C. K. Kim, B. K. Kim, H. M. Jeong, *Colloid Polym. Sci.* 1991, **269**, 895–900.

37 M. Pospíšila, P. Čapkováa, D. Měřínskáb, Z. Maláčb, J. Šimoníkb, J. *Colloid Interface Sci.* 2001, **236**, 127-131.

38 T. D. Fornes, P. J. Yoon, H. Keskkula, D. R. Paul, *Polymer,* 2001, **42**, 9929-9940.

39 A. Pattanayak, S. C. Jana, *Polymer,* 2005, **46**, 3394-3406.

40 G. Lligadas, J. C. Ronda, M. Galià, V. Cádiz, *Biomacromolecules,* 2007, **8**, 686–692.

41 T. W. Pechar, G. L. Wilkes, B. Zhou, N. Luo, *J. Appl. Polym. Sci.,* 2007, **106**, 2350–2362.

42 B. X. Fu, W. Zhang, B. S. Hsiao, M. Rafailovich, J. Sokolov, G. Johansson, et al., *High. Perform. Polym.* 2000, **12**, 565–571.

43 Y. S. Lu, R. C. Larock, *Biomacromolecules,* 2008, **9**, 3332-3340.

44 G. Lligadas, J. C. Ronda, M. Galia, V. Cadiz, *Biomacromolecules,* 2006, **7**, 3521–3526.

45 C.H. Wang, Y.T. Shieh, S. Nutt, *J. Appl. Polym. Sci.,* 2009, **114**, 1025–1032.

46 X. Cao, Y. Habibi, L. A. Lucia, *J. Mater. Chem.* 2009, **19**, 7137-7145

47 S. H. Choi, Y. J. Kim, S. Kim, C. Kim, *Polymer,* 2004, **45**, 6045-6057.

48 J. Feng, C.-M. Chan, *Polymer,* 1997, **38**, 6371–6378.

49 J. T. Garrett, R. Xu, J. Cho, J. Runt, *Polymer,* 2003, **44**, 2711–2719.

50 L. Rueda, A. Saralegui, B. Fernández d'Arlas, Q. Zhou, L. A. Berglund, M. A. Corcuera, I. Mondragona, A. Eceiza, *Carbohydr. Polym.,* 2013, **92**, 751–757.

51 Y. Xia, R. C. Larock, *Polymer,* 2010, **51**, 2508.

52 S. Turri, M. Levi, *Macromolecules,* 2005, **38**, 5569–5574.

53 S. F. Edwards, H. Takano and E. M. Terentjev, *J. Chem. Phys.*, 2000, **113**, 5531 – 5538.

54 F. M. Uhl, S. P. Davuluri, S. C. Wong, D. C. Webster, *Chem. Mater.,* 2004, **16**, 1135–1142.

55 L. W. Wang, T. Ye, H. Y. Ding, J. D. Li, *Eur. Polym. J.,* 2006*,* **42**, 2921–2930.

56 I-K. Yang, P-H. Tsai, *Polymer,* 2006, **47**, 5131–5140.

57 K. M. Lee, C. D. Han, *Macromolecules,* 2003, **36**, 804–815.

58 S. Choi, K. M. Lee, C. D. Han, *Macromolecules,* 2004, **37**, 7649-7662.

59 F. K. Li, R. C. Larock*, J. Polym. Sci. Part B: Polym. Phys.* 2001,**39**, 60-77.

60 H. C. Kuan, H. Y. Su, C. C. M. Ma, *J. Mater. Sci.* 2005, **40**, 6063-6070.

61 B. Finnigan, K. Jack, K. Campbell, P. Halley, R. Truss, P. Casey, D. Cookson, S. King, D. Martin, *Macromolecules*, 2005, **38**, 7386–7396.

62 H. Y. Choi, C. Y. Bae, B. K. Kim, *Prog. Org. Coat.,* 2010, **68**, 356–362.

List of Schemes

List of Figures

List of Tables

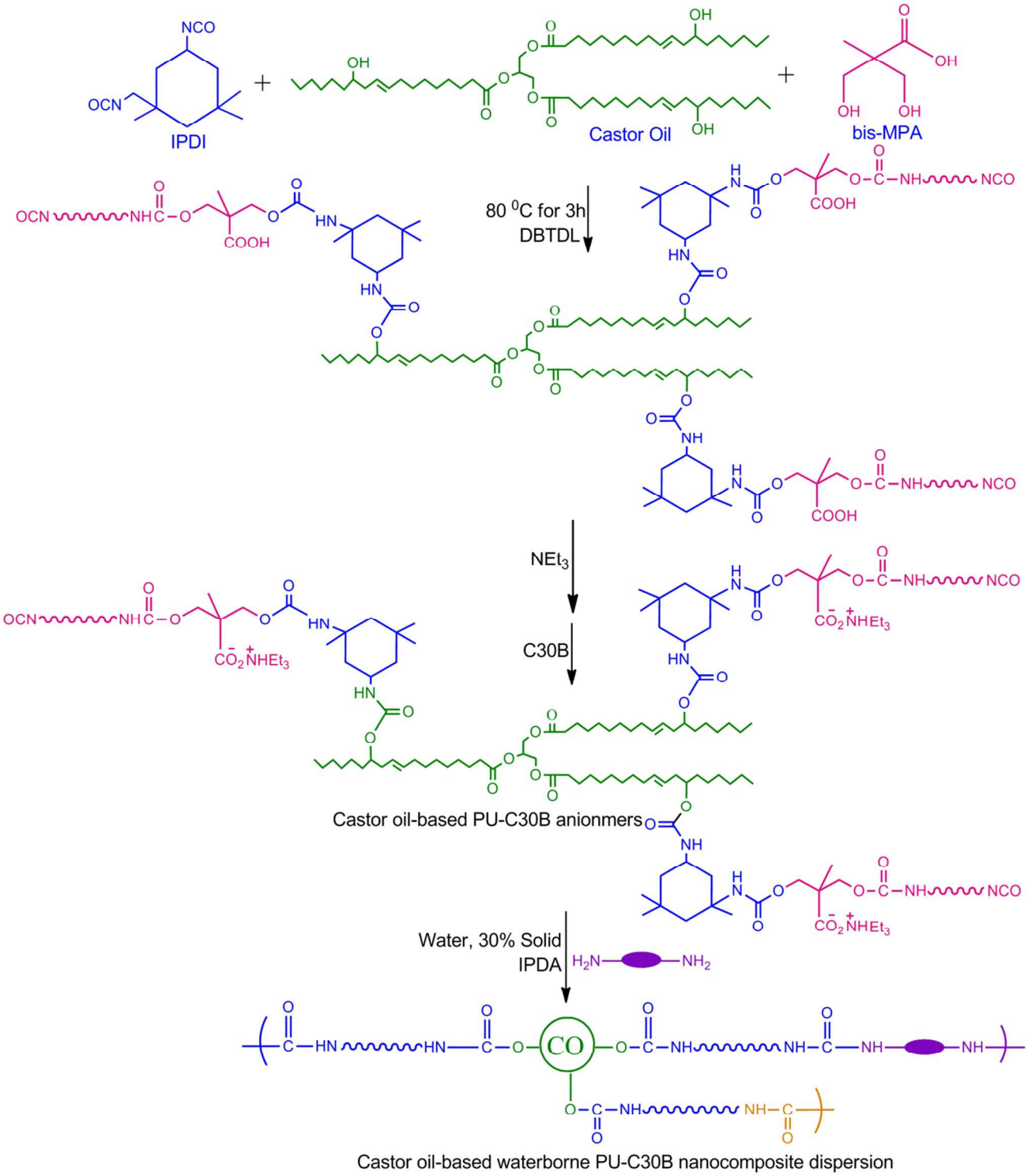

Scheme 1 Synthesis of castor oil-based WPU-C30B nanocomposites.

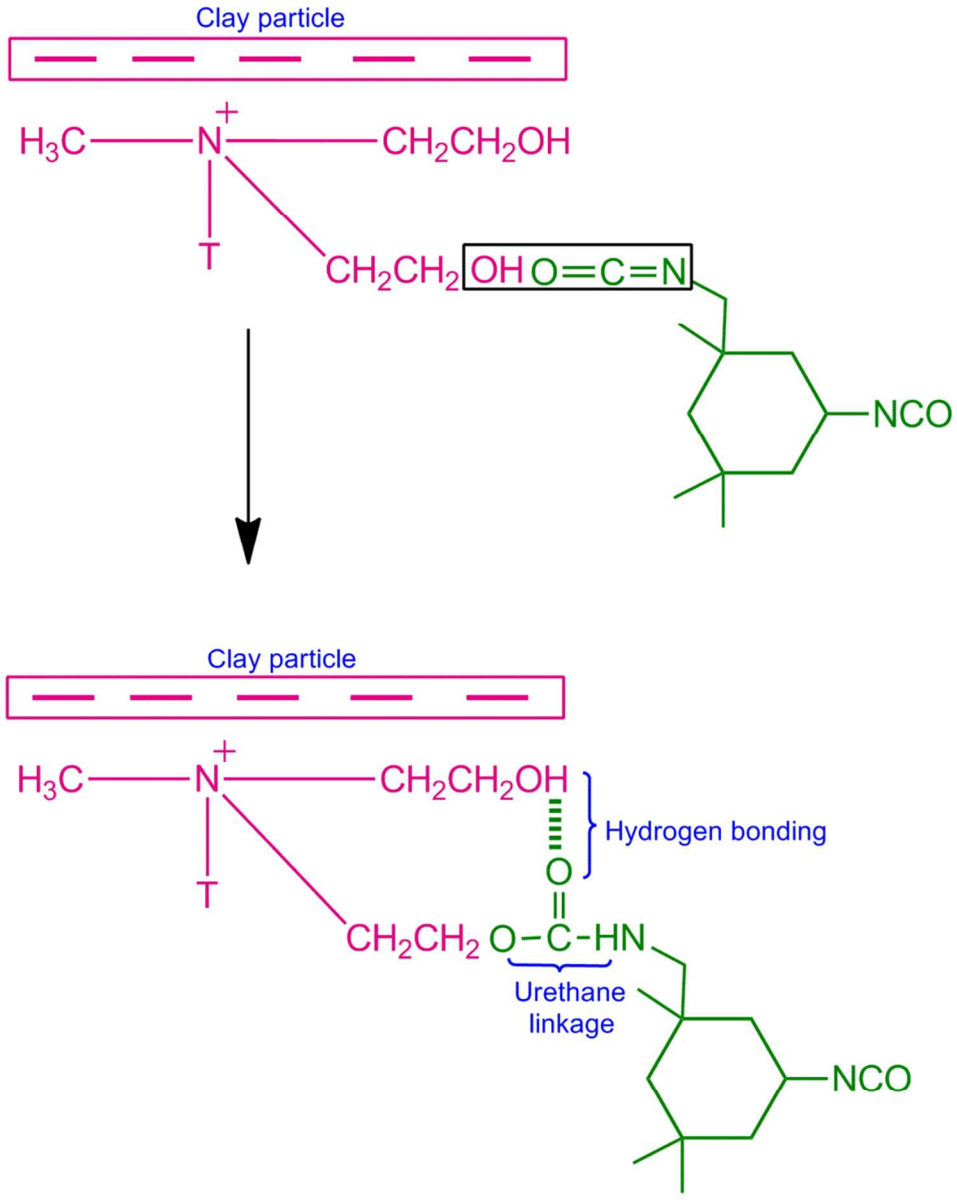

Scheme 2 The probable hydrogen bonding present in the WPU and C30B.

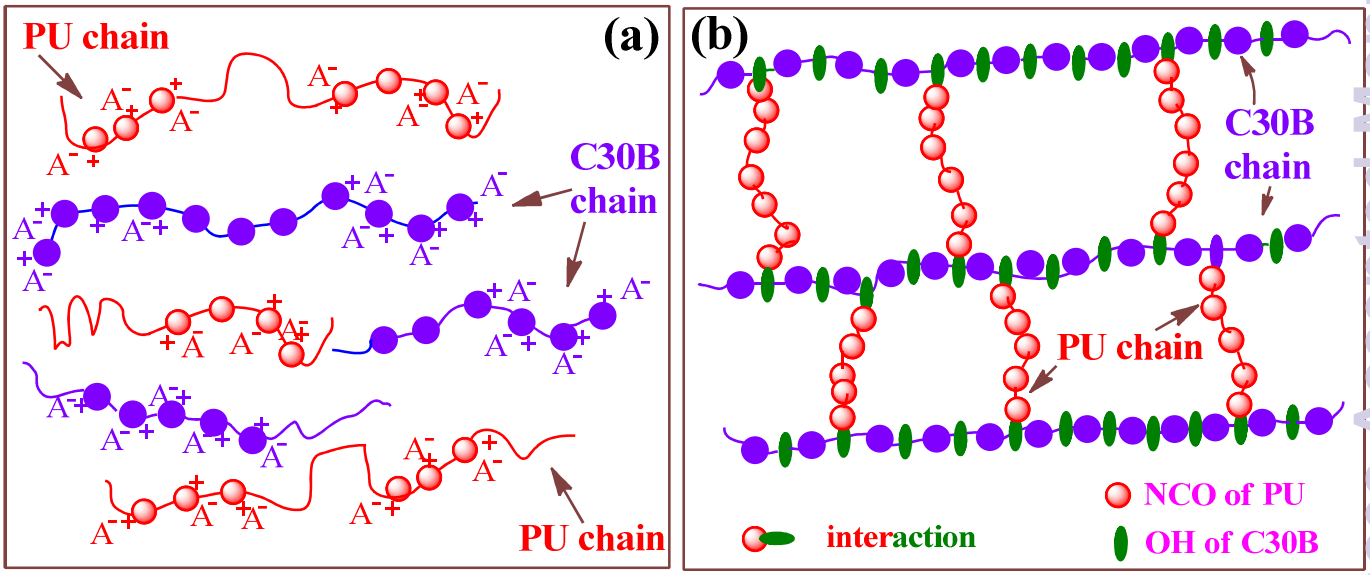

Scheme 3 (a) Electrostatically stabilized PU-C30B nanocomposites dispersion. (b) PU back-bone modification by C30B in non-aqueous solvents by physical interaction or grafting.

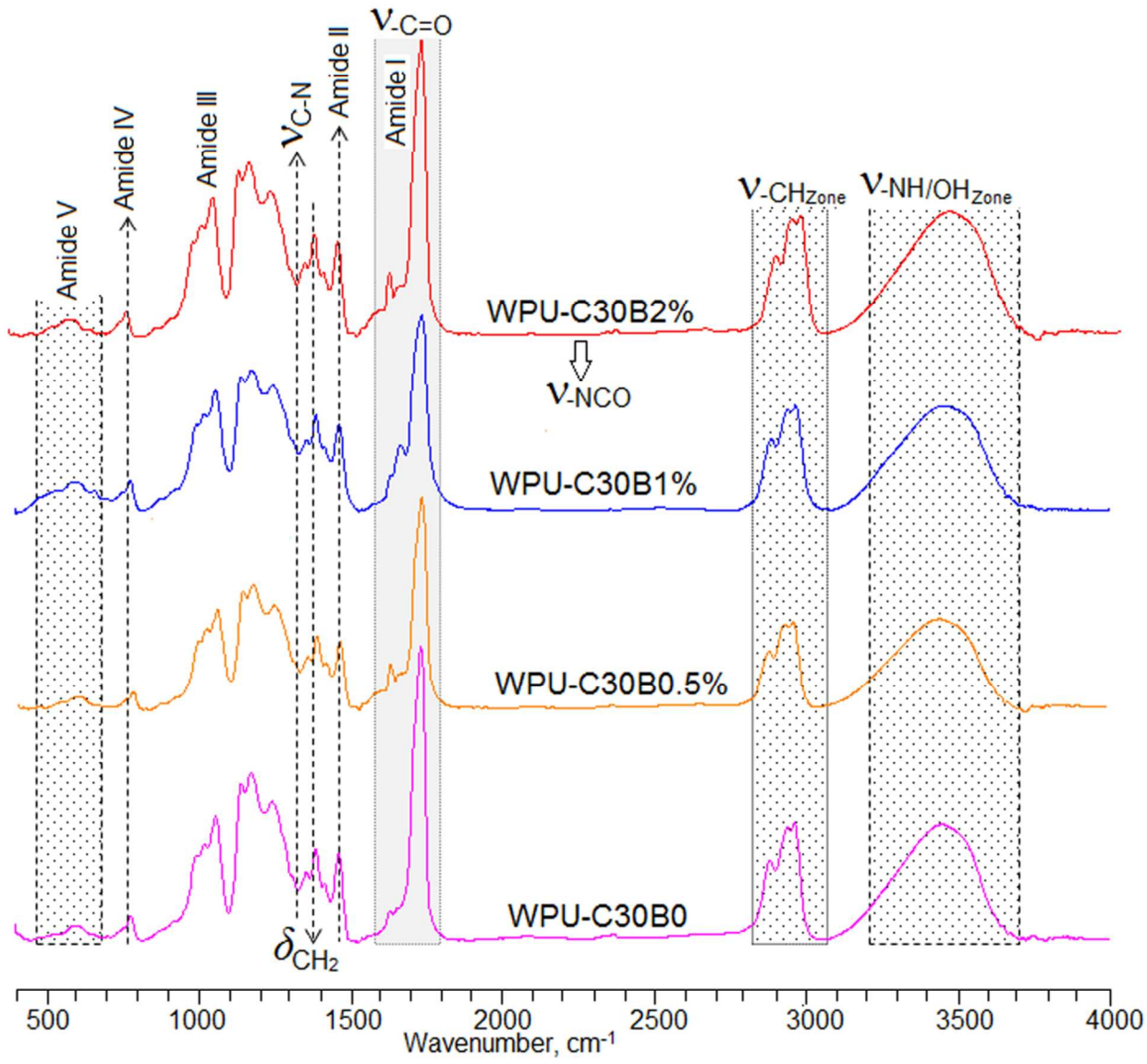

Fig. 1 FT-IR spectra of WPU-C30B0 and its WPU-C30B nanocomposites with different content of C30B.

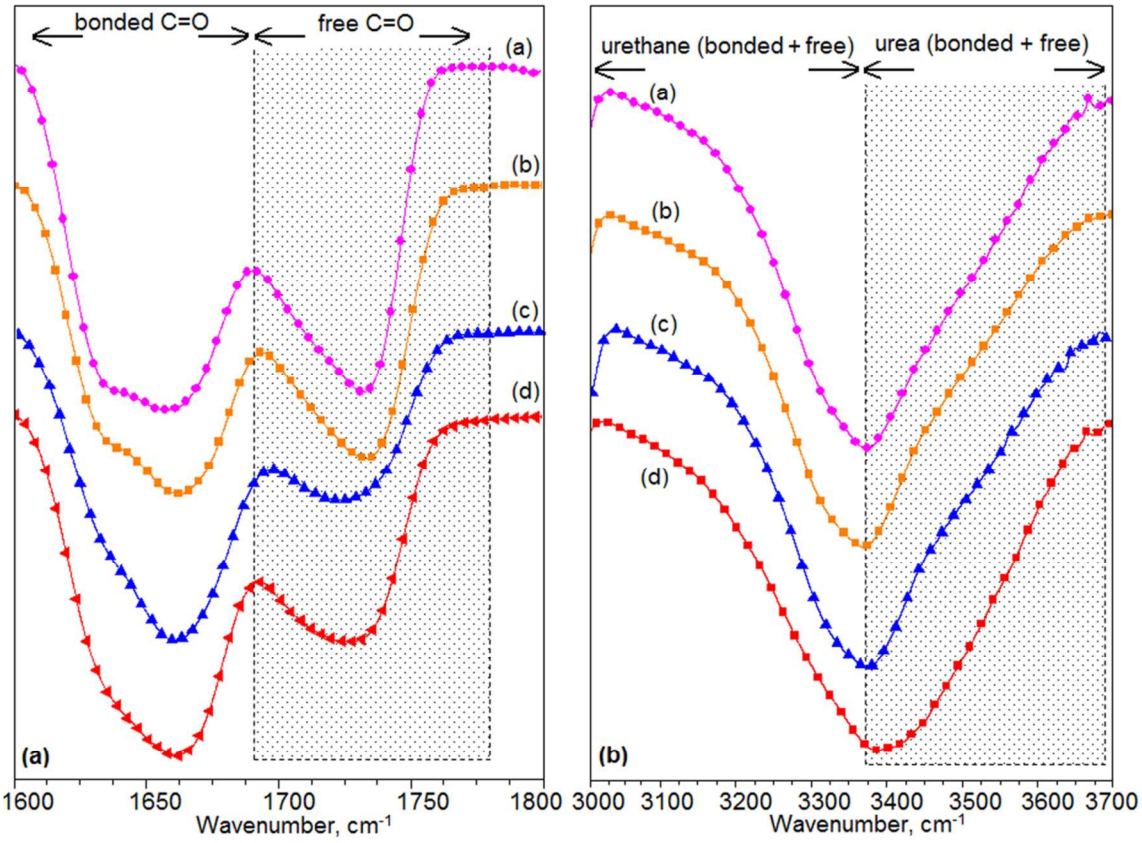

Fig. 2 (a) Carbonyl stretching (–C=O) and (b) amide (–N–H) zone of different WPU-C30B nanocomposites: (a) WPU-C30B0, (B) WPU-C30B0.5%, (c) WPU-C30B1%, and (d) WPU-C30B2%.

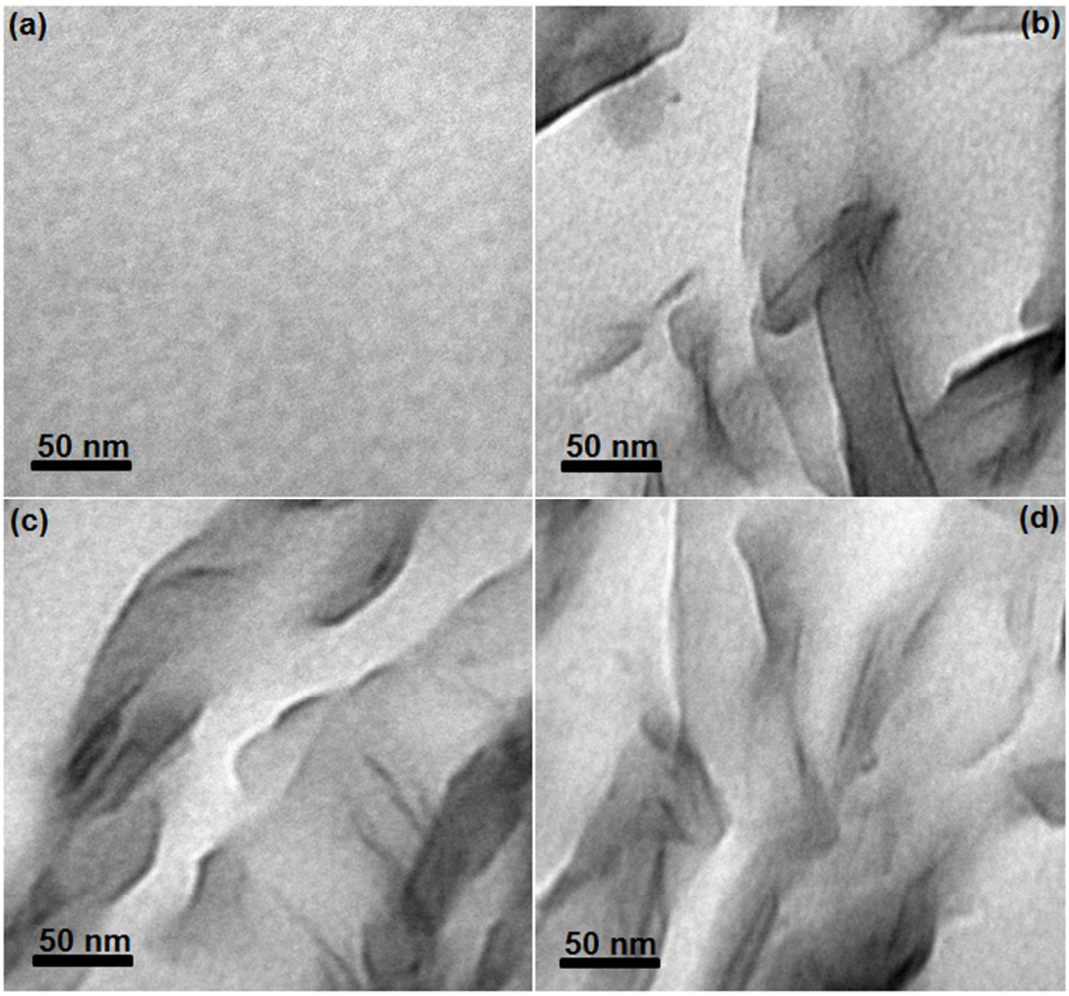

Fig. 3 TEM images of (a) WPU-C30B0, (B) WPU-C30B0.5%, (c) WPU-C30B1%, and (d) WPU-C30B2%.

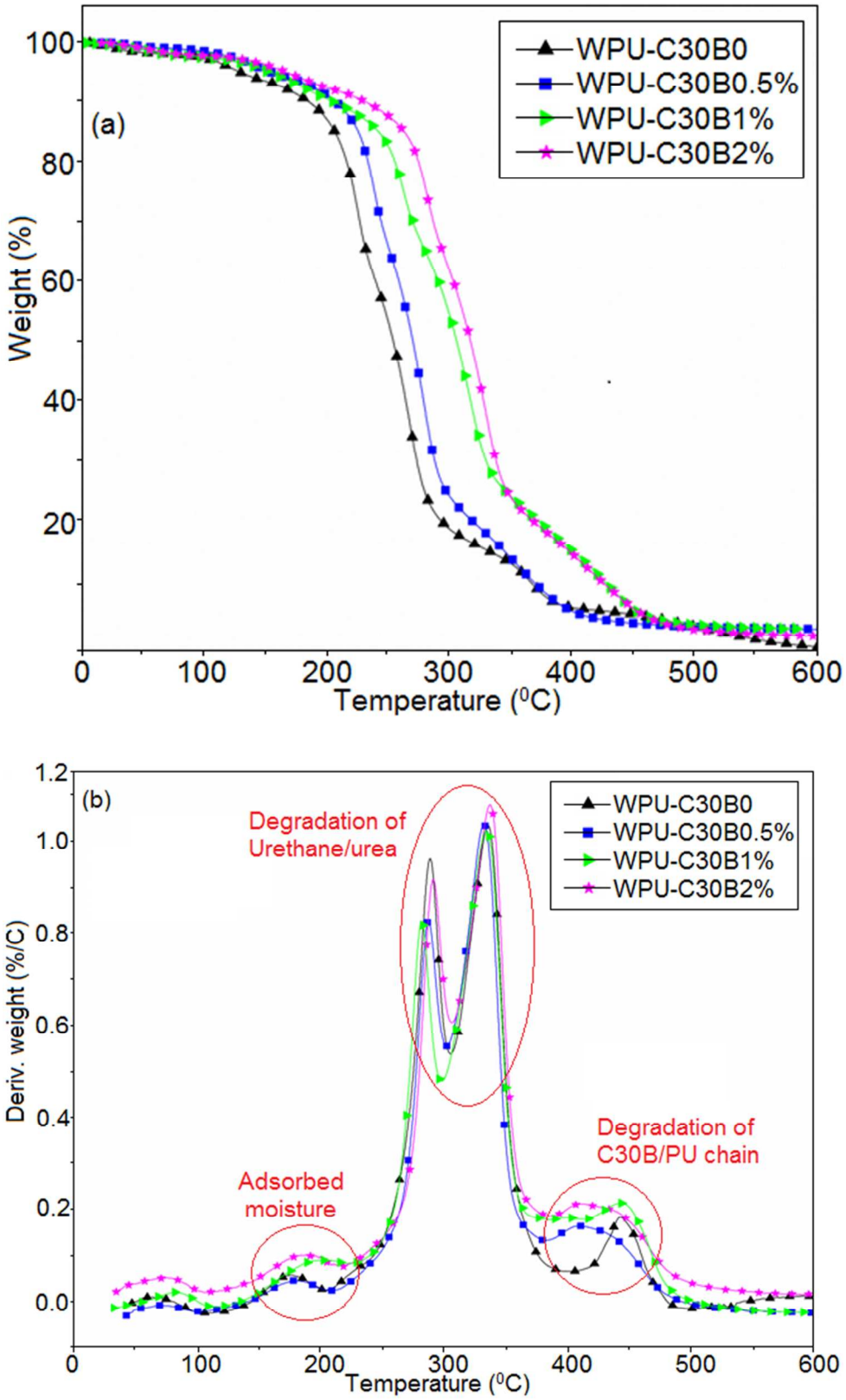

Fig. 4 The (a) TGA and (b) DTG curves of WPU-C30B nanocomposites.

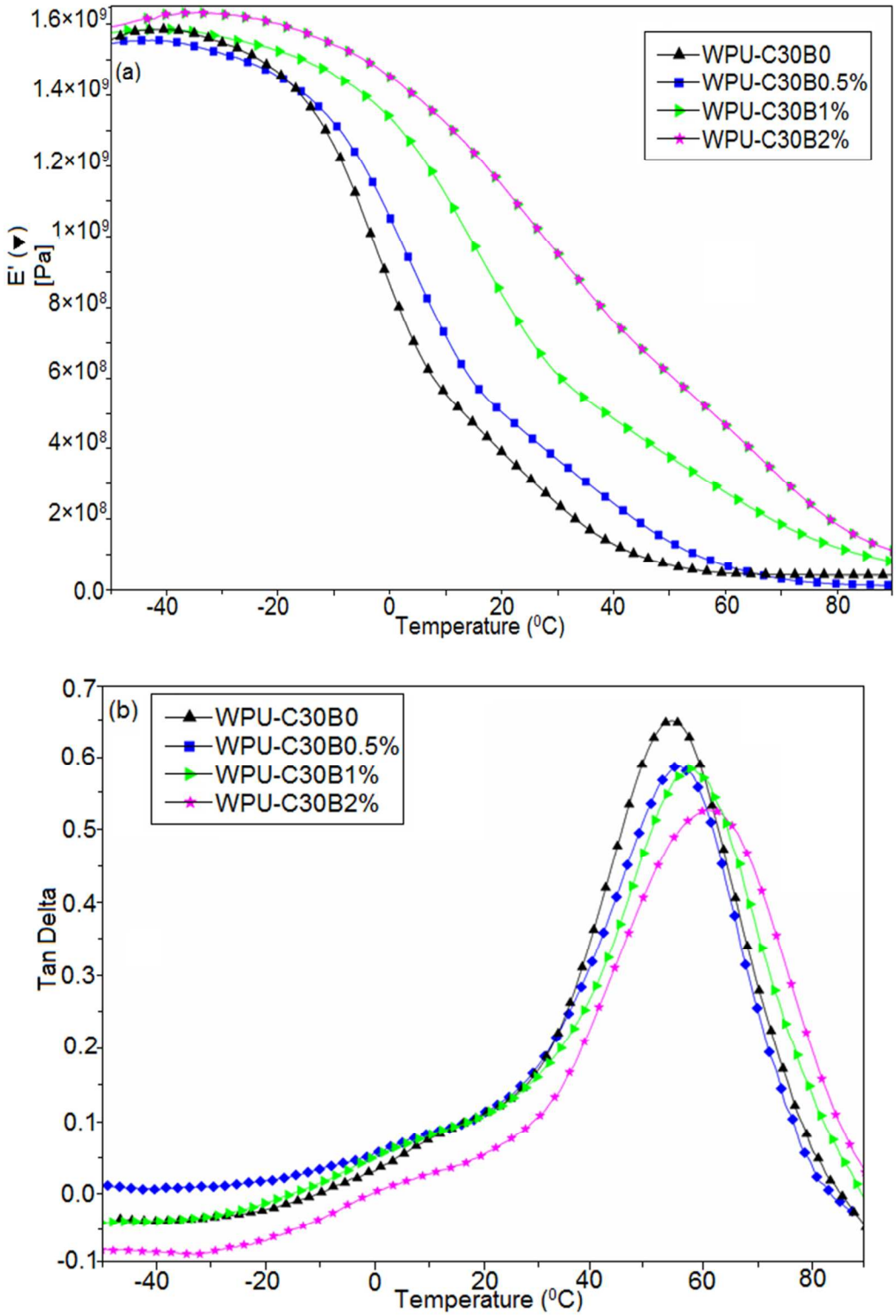

Fig. 5 The (a) storage modulus (E') and (b) loss factor (tan δ) as a function of temperature for the WPU-C30B nanocomposites.

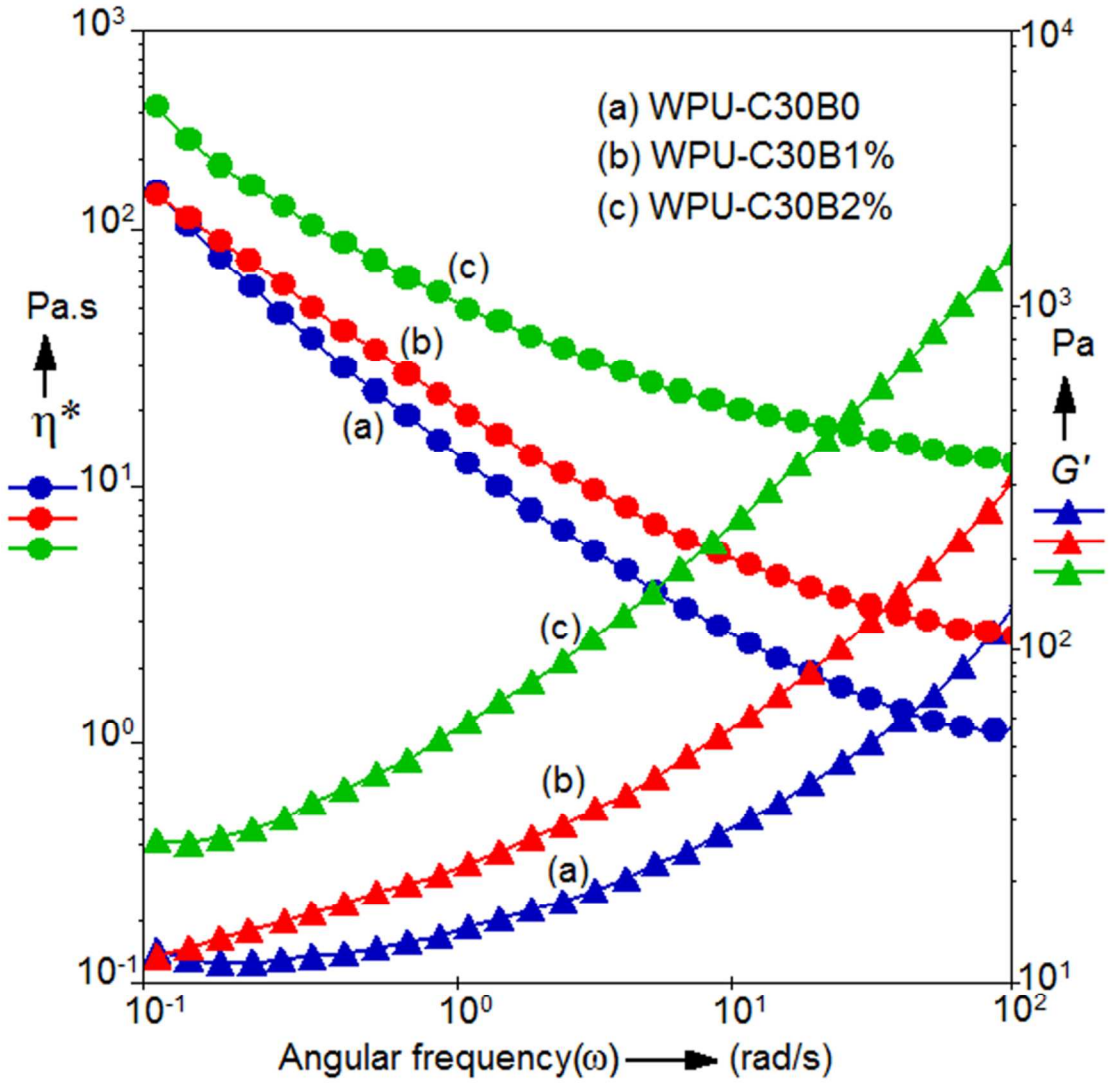

Fig. 6 Angular frequency dependence of complex viscosity ($|\eta^*|$) and storage modulus (G') of WPU-C30B nanocomposites.

Table 1 DMTA and DSC for the WPU-C30B nanocomposites

Sample code	T_g (DMTA) (^oC)	E' at (40 ^oC) (MPa)	E'at (T_g+5 ^oC) (MPa)	Tanδ_{max}	T_g (DSC) (^oC)	$\upsilon_c \times 10^{-4}$ (kg/m^3) at (40 ^oC)	$\upsilon_c \times 10^{-3}$ (kg/m^3) at (T_g+5 ^oC)
WPU-C30B0	53.1	409	29.9	0.8	25.1	4.2	3.5
WPU-C30B0.5%	56.3	521	26.2	0.6	39.5	5.6	2.8
WPU-C30B1%	58.9	149	63.7	0.5	41.2	14.8	0.8
WPU-C30B2%	63.1	176	28.1	0.4	42.0	17.4	2.8

Table 2 Thermal and mechanical properties of the WPU-C30B and its nanocomposites with different content of C30B

Sample code	Tensile strength (MPa)	Young's Modulus (MPa)	Elongation at break (%)	TGA data [^{o}C]			
				T_{10} (^{o}C)	T_{50} (^{o}C)	T_{max} (^{o}C)	%, wt remaining at 450 ^{o}C
WPU-C300	16.7	22.3	343.7	249.2	325.7	319.7	5.1
WPU-C30B0.5%	19.1	44.8	312.2	263.5	337.4	322.4	4.8
WPU-C30B1%	25.8	52.5	266.1	264.1	346.0	336.1	6.1
WPU-C30B2%	27.9	134.8	144.8	271.1	351.1	338.6	6.6

Effect of reactive organoclay on physicochemical properties of vegetable oil-based waterborne polyurethane nanocomposites

T. Gurunathan[1,2,*] Smita Mohanty[1,2,] Sanjay K. Nayak[1,2]

[1]Advanced Research School for Technology and Product Simulation (ARSTPS), Central Institute of Plastics Engineering & Technology, Guindy, Chennai - 600032, India

[2]Laboratory for Advanced Research in Polymeric Materials (LARPM), Central Institute of Plastics Engineering and Technology, Bhubaneswar -751024, India

Address correspondence to:

T. Gurunathan,

Central Institute of Plastics Engineering & Technology, Guindy, Chennai - 600032, India

E-mail: jguru001@gamil.com

Graphical Abstract